Surface & Coatings Technology 206 (2011) 354–359

Contents lists available at ScienceDirect

Surface & Coatings Technology

journal homepage: www.elsevier.com/locate/surfcoat

Structural, mechanical and electrical-contact properties of nanocrystalline-NbC/amorphous-C coatings deposited by magnetron sputtering

Nils Nedfors [a,*], Olof Tengstrand [b], Erik Lewin [a,1], Andrej Furlan [a], Per Eklund [b], Lars Hultman [b], Ulf Jansson [a]

[a] Department of Materials Chemistry, Uppsala university Regementsvägen 1 SE-752 35 Uppsala, Sweden
[b] Department of Physics, IFM, Linköping University, SE-581 83 Linköping, Sweden

ARTICLE INFO

Article history:
Received 10 November 2010
Accepted in revised form 11 July 2011
Available online 20 July 2011

Keywords:
Nanocomposite
Niobium carbide
Electrical contact properties
Mechanical properties
Magnetron sputtering

ABSTRACT

Niobium-carbide nanocomposite coatings with a carbon content varying from 43 to 64 at.% were deposited by dual DC magnetron sputtering. X-ray diffraction, x-ray photoelectron spectroscopy and electron microscopy showed that all coatings consisted of nanometer sized NbC grains embedded in a matrix of amorphous carbon. Mechanical properties and electrical resistivity showed a strong dependency on the amount of amorphous carbon (a-C) and NbC grain size in the coating. The highest hardness (23 GPa), elastic modulus (295 GPa) and the lowest resistivity (260 μΩ cm) were measured for the coating with about 15% of a-C phase. Contact resistance measurements using a crossed cylinder set-up showed lowest contact resistance for the coating containing 33% a-C (140 μΩ at a contact force of 100 N), which is comparable to a Ag reference (45 μΩ at a contact force of 100 N). Comparison with TiC-based nanocomposites studied under similar conditions showed that the Nb–C system has less tendency to form a-C and that lowest contact resistance is obtained at comparable amounts of a-C phase in both material systems (33% for Nb–C compared to 35% for Ti–C). With these good electrical contact properties, the Nb–C nanocomposites can be considered as a potential material for electrical contact applications.

1. Introduction

Electrical contacts can be found in a wide variety of applications in today's electrified society. A good electrical contact transfers electrical current between two conductors with a minimum of energy loss and should also have good corrosion and wear resistances. Traditionally, contact materials are coated with a soft noble metal resulting in low electrical contact resistance but poor wear resistance and increased costs. These contact materials are not suitable for sliding contacts and there is therefore a need for new materials that can sustain wear and retain the low contact resistance of the noble metals.

An alternative type of contact material is ceramic binary and ternary nanocomposites such as Ti–C and Ti–Si–C [1–3]. Typically, these nanocomposites consist of nanocrystalline metal carbide (nc-MeC) in an amorphous matrix of, e.g., carbon (a-C) or SiC (a-SiC). The great potential of this type of coatings is their design possibilities; the material properties of the coatings can be controlled by the microstructure (grain size and matrix thickness) and also by the choice of transition metal (Me) [1–14]. The simplicity of binary nanocomposite coatings makes them an interesting alternative to ternary nanocomposites, especially when studying the microstructure and its connection to the properties of the coating for different transition metals. Earlier studies have shown that magnetron sputtered nc-TiC/a-C nanocomposite coatings have excellent electrical contact properties for contact applications [2,15,16]. However, TiC oxidizes in rough environments, which would have a detrimental effect on the long-time contact properties of this materials.

Preliminary results from Lewin show that nc-ZrC/a-C nanocomposite coatings have poor contact resistance most likely due to the formation of very small grains with a high amount of a poorly conducting matrix phase of amorphous carbon [16]. In contrast, it was observed that nc-NbC/a-C coatings could give excellent properties potentially exceeding those of nc-TiC/a-C [16]. We have performed a more detailed investigation of a series of nc-NbC/a-C coatings with varying carbon content synthesized in a DC magnetron sputtering system. The coatings were characterized with respect to microstructure as well as electrical and mechanical properties in order to investigate how the microstructure of the coating influences the performance in an electrical contact application.

2. Experimental

Nb–C coatings were deposited in an ultra high vacuum chamber (base pressure of 10^{-8} Pa) by nonreactive unbalanced DC-magnetron sputtering from two separate 2 inch elemental targets supplied by Kurt J Lesker Ltd (Nb 99.95% pure and C 99.999% pure). The magnetrons were directed towards a rotating substrate holder at a distance of 15 cm. The Ar-plasma was generated at a constant pressure of 0.4 Pa

* Corresponding author. Tel.: +46 18 4713738; fax: +46 18 513548.
E-mail address: nils.nedfors@mkem.uu.se (N. Nedfors).
[1] Present address: Laboratorz of Nanoscale Materials Science, Empa, Überlandstrasse 129, CH-8600 Dübendorf, Switzerland.

0257-8972/$ – see front matter © 2011 Elsevier B.V. All rights reserved.
doi:10.1016/j.surfcoat.2011.07.021

(3.0 mTorr) and with an Ar gas flow rate of 45 sccm. The substrates were biased to −50 V. Coatings with a carbon content between 43 and 64 at.% were deposited through tuning of the Nb-magnetron current from 140 mA down to 60 mA. The current to the C-magnetron were kept constant at 300 mA through all depositions. The thicknesses of the coatings were 0.5 μm–0.7 μm.

Single-crystal Si(001) (10×10 mm^2) substrates were used for composition analysis, phase analysis and electrical resistivity measurements. Contact resistance measurements on flat surfaces give unreliable results and we have therefore used Ni-plated Cu cylinders (20 mm in length, 10 mm in diameter) as a substrate for contact resistance measurements. Composition and phase analysis were also performed on the cylinder substrates to compare composition and microstructure for the coatings deposited on different substrates. The Si substrates were placed in the center of the substrate holder while the cylinder substrates where situated 20 mm out from the center during deposition. The substrates were kept at a constant temperature of 300 °C by a heater wire integrated in the substrate holder. The substrates were preheated for at least 45 min and the targets were presputtered for at least 10 min before deposition.

The chemical composition of the coatings was determined with X-ray photoelectron spectroscopy (XPS) using a Physical Systems Quantum 2000 spectrometer with monochromatic Al Kα radiation. Energy calibration was carried out with Au and Ag reference samples and the sensitivity factors, given by Physical Electronics Inc. software MultiPak V6.1A, were used for quantitative analysis [17]. Depth profiles of the coatings were acquired by rastered Ar^+-ion sputtering over an area of 1×1 mm^2 with ions having energy of 500 eV. High resolution XPS C1s spectra were acquired after 30 min of Ar^+-ion sputter etching over an area of 1×1 mm^2 with ions having energy of 500 eV. The XPS analysis area was set to a diameter of 200 μm in all measurements. Grazing incidence (GI) x-ray diffraction (XRD) measurements were carried out on a Siemens D5000 using Cu Kα radiation and parallel beam geometry with a 2° incidence angle. The cell parameters were calculated from the GI-XRD diffractograms. Microscopy studies were carried out on selected coatings, using a Zeiss LEO 1550 scanning electron microscopy (SEM) and a FEI Tecnai G2 TF 20 UT field emission gun transmission electron microscopy (TEM) operated at a 200 keV acceleration voltage. The cross sectional TEM samples were made by mechanical polishing to a thickness of ~50 μm. After this the samples were ion milled in a Gatan Precision Ion Polishing System (PIPS), using Ar^+ ions with energy of 5 keV. As a final step, the samples were polished using 2 keV Ar^+ ions. A Wyko NT1100 optical profiler from Veeco was used to determine the surface roughness of the coatings in terms of the root-mean-squared (RMS) value. Mechanical properties were obtained using CSM Instruments nano-indenter XP with a diamond Berkovich tip. Load–displacement curves were acquired with an indentation depth set to 50 nm, a loading rate of 3 mN/min and about 20 indents per sample. Hardness and elastic modulus were determined by the Oliver–Pharr method. Electrical resistivity of the coatings was acquired by the four-point-probe measurement technique using equipment from Veeco Instruments Inc. The contact resistance of the coatings was determined using a custom-built set-up with a crossed cylinder geometry, which allowed the voltage drop over the contact interface to be measured as a function of contact force. A sketch of the crossed cylinder set-up can be found in [3]. All contact resistance measurements were made against an Ag-countercontact.

3. Results

3.1. Microstructure

The results show that the coatings are nanocomposites consisting of nanocrystalline NbC_x grains in an amorphous carbon matrix (see Sections 3.2 and 3.3 for the determination of NbC_x grains and amorphous carbon in the coatings). In the following this material will be described as nc-NbC/a-C. Fig. 1 shows SEM images of fractured cross-sections of two coatings with different carbon content. The most metal-rich coating (Fig. 1a) exhibits a columnar microstructure. As can be seen, the columnar structure is less prominent in the most carbon-rich coating (Fig. 1b). This trend with a reduced columnar structure at high carbon contents has also been observed in the nc-TiC/a-C system [5,14]. Fig. 2 shows cross-sectional TEM images of three coatings with different carbon content. The TEM images show a microstructure consisting of nanometer sized crystal grains embedded in an amorphous matrix. The microstructure is strongly dependent on the carbon content. The most metal-rich coating (Fig. 2a) has large crystalline grains within the columnar structure. The dark field image inset, obtained using segments of the (002) and (111) diffraction rings shows that the grains are elongated in the film growth direction. In contrast, the most carbon-rich coating exhibits more equiaxed grains, which are evenly distributed in the coating (Fig. 2c). It can also be seen in Fig. 2 that the size of the crystal grains is dependent on carbon content with an average size estimated to be 75 nm for the most metal-rich coating compared to grain sizes in the range 3 to 5 nm for the most carbon-rich coating. An optical profiler was used to analyze the surface roughness of the coatings deposited on Si(100). No trend could be seen for the RMS value, which varied from 1.5 nm for the coating containing 49 at.% C to 3.1 nm for the coating containing 54 at.% C.

3.2. X-ray diffraction

Fig. 3 shows diffractograms from the nc-NbC/a-C coatings with a carbon content ranging from 43 at.% to 64 at.% C. The peaks in the diffractograms can be assigned to NbC with a B1 (NaCl) structure. $\theta-2\theta$ scans (not shown here) showed a out-of-plane (111) texture in all the coatings. The texture is most distinct for the metal-rich coatings. No difference could be seen between the GI and $\theta-2\theta$ diffractograms in terms of peak position and peak broadening. The cell parameters for the NbC crystal grains obtained from the peak positions in the GI-XRD diffractograms range from 4.47 Å to 4.49 Å, which are slightly larger compared to values reported by Kempter et al. [18].

It can be seen in Fig. 3 that the diffraction peaks are broader for the most carbon-rich coatings. A similar behavior has been observed in other sputtered transition metal carbide systems such as TiC and was attributed to the grain size broadening effect [2,7,8]. The carbide grain sizes in the Nb–C coatings in Fig. 3 are estimated using the Scherrer equation [19]. However, since peak broadening can also be due to internal stresses, a Williamson–Hall plot can give a more accurate assessment [20]. Fig. 4 shows the size of the carbide grains estimated with both the Scherrer equation and Williamson–Hall plot. As can be seen, the calculations give large error bars for data points based on the Scherrer equation for the metal-rich coatings. The data points from

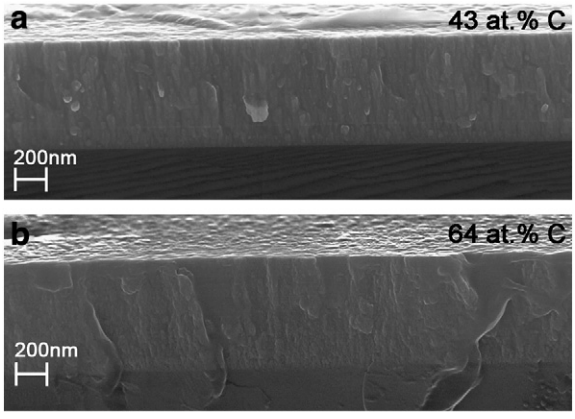

Fig. 1. Fractured cross-section SEM images of two coatings with different carbon content: a) 43 at.% C, b) 64 at.% C.

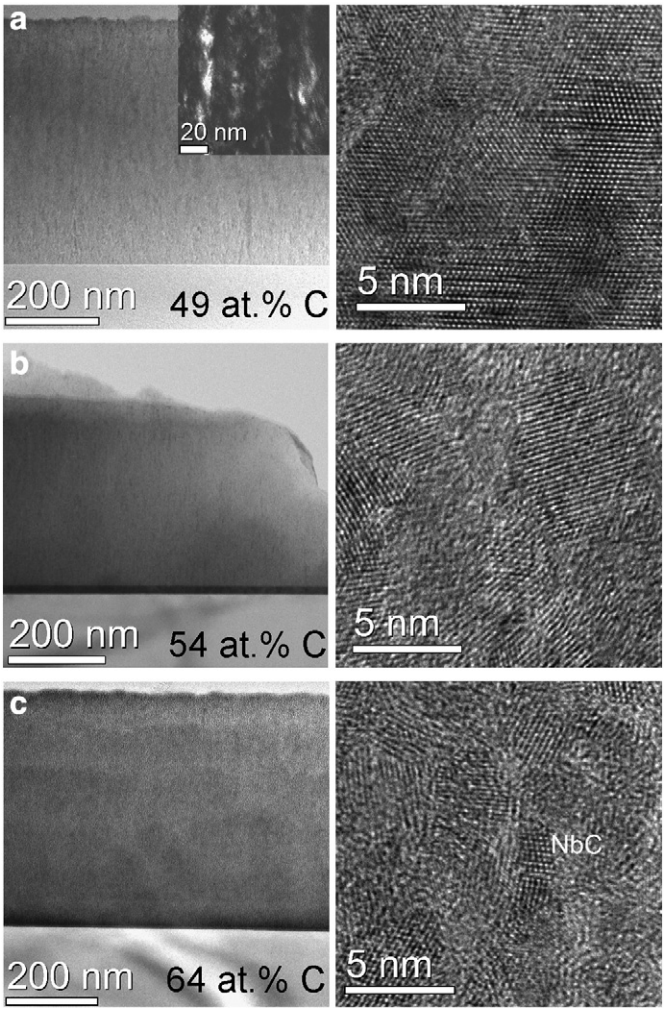

Fig. 2. Cross-sectional TEM images of three coatings with different carbon content: a) 49 at.% C, b) 54 at.% C, c) 64 at.% C. The images in the right column are the same coatings taken at a higher magnification. A crystal grain has been marked with NbC in c). Dark field image inset in a) obtained using the (002) and (111) reflections.

the Williamson–Hall plot of these coatings are excluded from Fig. 4 due to a too large variation in the FWHM of the diffraction peaks. While the grain size determination in Fig. 4 is in good agreement with the TEM results in Fig. 2 for the most carbon-rich coatings, the result reveals a large underestimation of grain sizes for the two most metal-rich coatings (~75 nm from TEM compared to 12 nm from Scherrer equation for the sample containing 49 at.% C). This can be explained by the anisotropy of the carbide grain shape observed for the metal-rich coatings in Fig. 2a. The Scherrer equation and the Williamson–Hall plots assume equiaxed grains and give erroneous results for anisotropic shapes. The results in Fig. 4 confirm the carbide grain size dependence with carbon content observed by TEM (see Section 3.1). The reduction in grain size at higher carbon contents is a trend also observed in other carbide-based nanocomposite systems (see, e.g., Zhang et al. [8]).

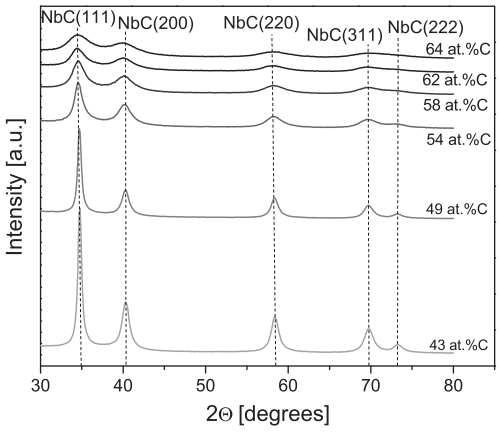

Fig. 3. GI X-ray diffractograms from Nb–C coatings with different carbon contents deposited by magnetron sputtering on Si(100) at 300 °C.

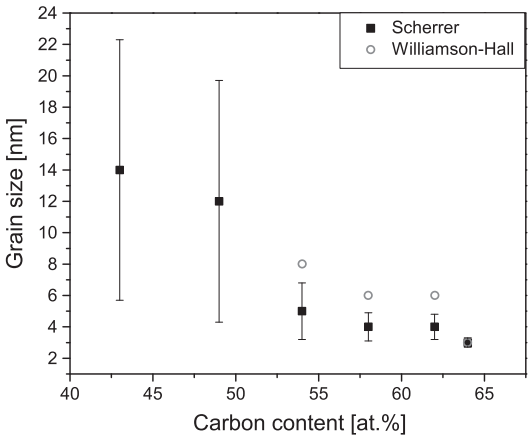

Fig. 4. Carbide grain diameters estimated from the Scherrer equation (squares) and Williamson–Hall plot (circles) for coatings with different carbon content.

3.3. X-ray photoelectron spectroscopy

Fig. 5 shows the C1s XPS peak of the coatings. Two separate features can be observed in the spectra. The peak at 284.4 eV is identified as carbon in the amorphous matrix (C–C bonds) [21]. The peak at 282.8 eV can be attributed to carbon in the niobium carbide (C–Nb bonds) although it is found at a slightly higher binding energy than reported by Ramqvist for bulk $NbC_{0.774}$ (282.0 eV) [22]. Consequently, in agreement with many other Me–C systems, these coatings consist of two phases: a nanocrystalline (nc) MeC_x phase in a matrix of amorphous carbon (a-C) [4,5,7–10,12,13]. By comparing the area of the two peaks in the C1s spectra, the relative amounts of the two phases (a-C and nc-NbC) can be determined. Fig. 6 shows that the relative amount of a-C phase increases with the total carbon content in the coating. The fact that we have 10–15% a-C in coatings with a total

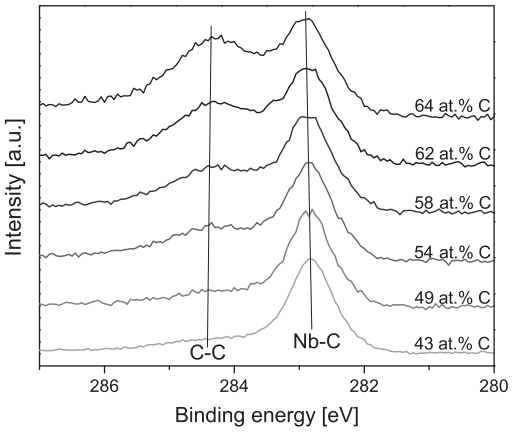

Fig. 5. XPS spectra of the C1s peak for Nb–C coatings with different carbon contents deposited by magnetron sputtering on Si(001) at 300 °C. Spectra acquired after sputtering with 500 eV Ar^+ ions to a depth of approximately 150 nm.

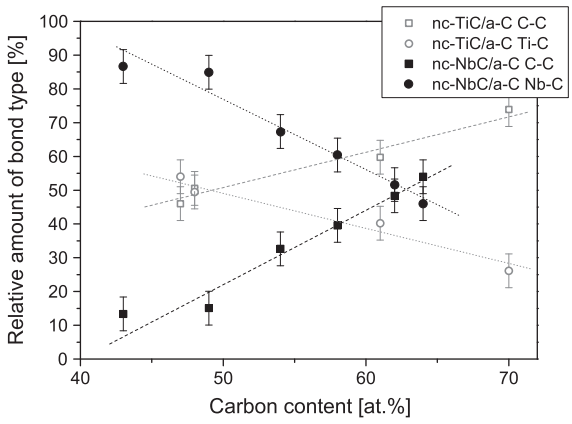

Fig. 6. The relative amount of the different bond types calculated from the XPS C1s spectra. The values for nc-TiC/a-C come from coatings deposited by DC magnetron sputtering under similar conditions by Lewin et al. [2]. Lines are only intended as guides for the eye.

carbon content less than 50 at.% strongly suggests that the NbC_x grains are substoichiometric. Included in Fig. 6 is also the relative amount of a-C phase in DC magnetron sputtered nc-TiC/a-C coatings studied by Lewin et al., see [2] for a detailed specification. It can be seen that nc-TiC/a-C coatings contain more a-C at a given carbon content; the reason behind this will be discussed under Section 4.1. Bulk XPS analysis (not shown here) shows that the relative amount of oxygen is around 1 at.% in all the coatings expect for the most metal-rich coating, which exhibits an oxygen content of approximately 5 at.%.

3.4. Mechanical properties

The hardness and elastic modulus of the Nb – C coatings, obtained from nano-indentation, are summarized in Figs. 7 and 8. In addition, data from nc-TiC/a-C coatings studied under similar conditions [16] are included in the figures. The hardness of the nc-NbC/a-C coatings varies from 23 GPa to 13 GPa, which is lower compared to the reported value of 27 GPa for NbC single crystal bulk sample [23]. The elastic modulus varies from 295 GPa to 162 GPa. In comparison the reported modulus value from single crystal bulk NbC sample is a factor two higher (500 GPa) [23]. Two things can be noted in Figs. 7 and 8; firstly a maximum can be seen for both the hardness and elastic modulus of the nc-NbC/a-C coatings at a total carbon content around 50 at.%. Such a maximum has been observed for nc-TiC/a-C by, e.g., Zehnder et al. [4]. Secondly, single crystal bulk NbC and TiC have similar hardness values (29 GPa and 27 GPa, respectively). This is not in agreement with the large differences in hardness values seen in Fig. 7 between Nb – C and Ti – C nanocomposites. The mechanism behind this discrepancy is discussed in Section 4.2.

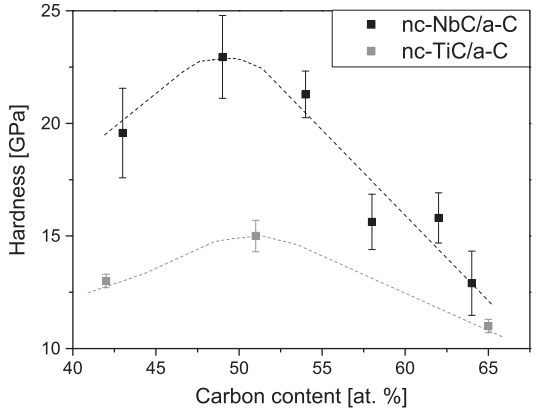

Fig. 7. Hardness values for coatings with different carbon content, obtained from nano-indentation. Data from DC magnetron sputtered nc-TiC/a-C coatings are included as a reference [16]. Lines are intended as guides for the eye.

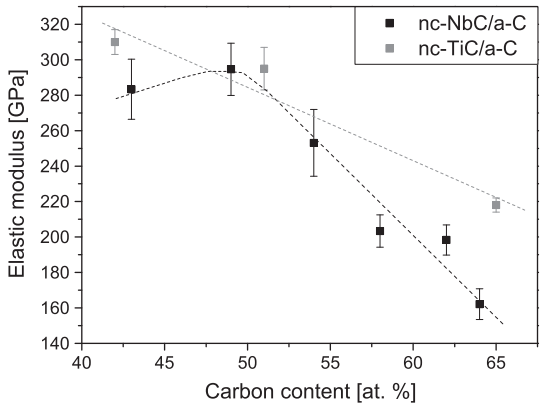

Fig. 8. Elastic modulus values for coatings with different carbon content, obtained from nano-indentation. Data from DC magnetron sputtered nc-TiC/a-C coatings are included as a reference [16]. Lines are intended as guides for the eye.

3.5. Electrical properties

The electrical resistivity of the different coatings measured by four-probe-measurements is shown in Fig. 9. The two coatings with a carbon content below 50 at.% have a rather low resistivity (<300 μΩ cm) while the other coatings exhibit a rapid increase in resistivity with higher total carbon content (400–1200 μΩ cm). It can be seen in Fig. 9 that the resistivity for nc-TiC/a-C coatings studied under similar conditions [2] is higher for all carbon contents.

The contact resistance measured at different contact force of three different coatings against Ag is presented in Fig. 10. The Ag reference curve is the contact resistance of Ag against Ag and is used as a reference resistance in the figure. All the curves show a similar behavior with a decrease in contact resistance with the increase of contact force. This is not surprising, since the increase of the contact force will break surface oxides and smear the contact material resulting in larger conducting contact spots. The contact resistance at a contact force of 100 N is lowered from 550 to 140 μΩ when the carbon content is increased from 43 to 54 at.% (an increase from 18 to 38% a-C phase). When the carbon content is increased further to 64 at.% C (65% a-C phase) the contact resistance instead increases dramatically to 4020 μΩ (100 N contact force). This has been observed in other carbide systems and is discussed

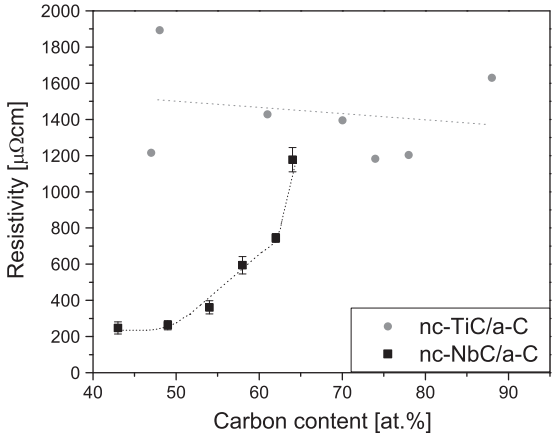

Fig. 9. Electrical resistivity for coatings with different carbon content, measured using the four point-probe technique. The resistivity values shown for nc-TiC/a-C coatings are measured by Lewin et al. under similar conditions [2]. Lines are intended as guides for the eye.

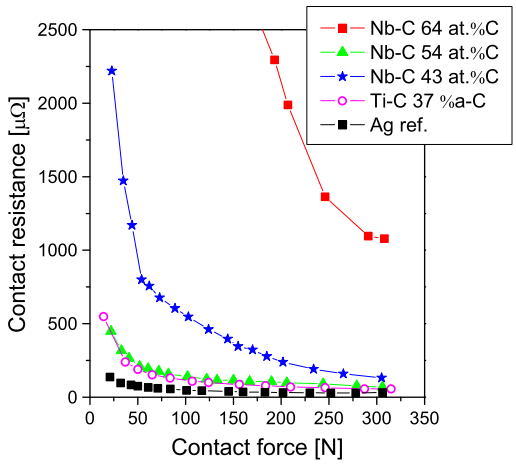

Fig. 10. Contact resistance at different contact force for coatings with different microstructure. Contact resistance for the Ti-C coating is measured by Lewin et al. under similar conditions [16]. Ag ref. is the contact resistance measured for silver against silver and intended as a reference. Lines are intended as guides for the eye.

in more detail in Section 4.2. It can also be seen that the contact resistance of the nc-NbC/a-C coating containing 54 at.% C (38% a-C) follows the curve of a magnetron sputtered nc-TiC/a-C coating (37% a-C) measured using the same type of crossed cylinder setup.

4. Discussion

4.1. Microstructure

The nc-NbC/a-C coatings exhibits a similar microstructural evolution with increasing carbon content as other binary nanocomposites deposited by magnetron sputtering [2,5,16]. As the a-C phase becomes accumulated in the column boundaries, it percolates the columns and encapsulates the grains (see Fig. 2a–c). Also, the grain size of the NbC grains decreases with higher carbon contents. This is also observed in other nc-MeC/a-C systems [2,4,7,8]. Furthermore, the most metal-rich coatings have anisotropic grains elongated in the growth direction while the most carbon-rich coatings exhibit equiaxed grains. Another interesting observation is that NbC_x grains are substoichiometric. Analysis of XPS data shows that the coatings in this study have NbC_x grains with x ranging from 0.66 to 0.84. Similar type of substoichiometric structures has earlier been observed for other magnetron sputtered nanocomposites [11,12] including nc-TiC_x/a-C coatings for x ranging from 0.44 to 0.64 [2]. It could be argued that thermodynamics should require a stoichiometric composition of the carbide in a two-phase nc-MeC/a-C coating. However, these coatings are deposited by magnetron sputtering at low temperatures in conditions far from equilibrium making it possible for a two-phase coating, with carbide grains deviating from equilibrium composition, to form.

A very important feature of the coatings is the thickness of the amorphous carbon phase (a-C). A rough estimation of the thickness can be obtained by using a cube model where the carbide grains are represented by equally sized cubes placed on the nodes of a three-dimensional cubic mesh (see Zehnder et al. [4] for a detailed description of the method). Grain sizes estimated from the XRD measurements (using the Williamson–Hall method) together with the relative amount of NbC_x and a-C phase obtained from XPS measurements and tabulated values for density and molar weight for respectively element were used to calculate the cube separation. A slightly modified model was used for the two coatings containing 43 and 49 at.% C taking into account the anisotropy of the carbide grain shape by using rectangular cuboids instead of cubes ten times longer in the *z* direction than in the *x* and *y* directions. Grain sizes were estimated from TEM images (100 nm and 75 nm for the coatings containing 43 and 49 at.% C respectively) instead of XRD for these two samples due to the erroneous grain sizes calculated using the Williamson–Hall method for these two coatings. Fig. 11 shows the estimated matrix thicknesses for the different coatings. It amounts to a few atomic layers on average in all coatings. Furthermore, the results suggest no large increase in the matrix thickness with higher carbon contents. This means that high amount of free carbon observed in the carbon-rich coatings in Fig. 5 is due to reduced grain sizes, which require a larger amount of amorphous matrix phase surrounding the carbide grains. Included in Fig. 11 is also the matrix thickness for nc-TiC/a-C coatings calculated using the same cube model by Lewin et al. [2]. It can be seen that the a-C matrix in the nc-TiC/a-C is considerably thicker compared to the nc-NbC/a-C coatings. It should be noted that the matrix thickness in Fig. 11 is an average thickness based on a cube model.

Both the difference in stoichiometry and matrix thickness between the Nb–C and Ti–C coatings can be explained by considering equilibrium phase diagrams. The energy cost to form a carbon vacancy in a transition metal carbide (Me) is reflected in the homogeneity range for MeC in a Me-C phase diagram. NbC has a homogeneity range of 42–50 at.% C while TiC has a wider homogeneity range of 35–49 at.% C [24]. This implies a lower energy cost to form a carbon vacancy in TiC compared to NbC and thereby more favorable to form substoichiometric TiC_x in a nc-TiC/a-C coating than substoichiometric NbC_x in a nc-NbC/a-C coating. Consequently, more free carbon atoms may cluster between the carbide grains and form bonds during growth in the nc-TiC/a-C coatings in comparison to the nc-NbC/a-C coatings and thereby resulting in a thicker a-C matrix in the nc-TiC/a-C coatings.

4.2. Properties of the coatings

The presence of an a-C phase surrounding the carbide grains will have a strong influence on the properties of the coatings. This is reflected in the hardness of the coatings presented in Fig. 7 where the more preserved columnar structure in the metal-rich coatings explains the higher hardness compared to the coatings containing more than 55 at.% C where the a-C matrix surrounds the carbide grains and thereby soften the coating further. Included in Fig. 7 are also hardness values for nc-TiC/a-C coatings measured under similar conditions by Lewin [16]. The hardness value is higher for all the nc-NbC/a-C coatings in comparison with the nc-TiC/a-C coatings at a given carbon content. An explanation for the difference in hardness can be the higher amount of a-C phase in the nc-TiC/a-C coatings, which allows the carbide grains in the coatings to glide and rotate to a larger extent resulting in softer coatings compared to the Nb–C based coatings. Fig. 8 shows a decrease in elastic modulus with the increase in carbon content (increase of a-C phase) for both the Nb–C and Ti–C based

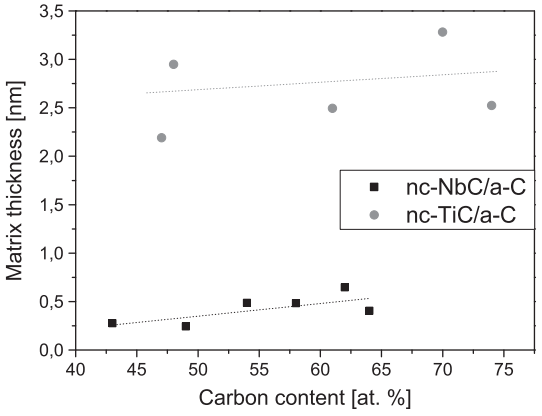

Fig. 11. Estimated thickness for the a-C phase for coatings with different carbon content. Included in the figure are also estimated thicknesses for the a-C in nc-TiC/a-C by Lewin et al. using the same model [2]. Lines are only intended as guides for the eye.

coatings. The ratio between the hardness and elastic modulus (H/E ratio) gives an indication of the wear resistance of a nanocomposite coating [25]. The H/E ratio of the nc-NbC/a-C coatings increases from 0.069 to 0.080 with the increase of carbon content compared to an increase from 0.042 to 0.050 for the nc-TiC/a-C coatings using the values for hardness and elastic modulus presented in Figs. 7 and 8. This suggests a better resistance to wear for nc-NbC/a-C coatings compared to nc-TiC/a-C coatings.

The electrical resistivity of the nc-NbC/a-C coatings (250–1200 μΩ cm) shown in Fig. 9 is in the same range as values published by Benndorf et al. [10] for Nb-containing a-C:H coatings. The amount of NbC|a-C interfaces per unit length is increased as the carbide grain size is decreased in the coatings, which can explain why the total resistivity in the coatings is increasing with the increase in carbon content. Resistivity values for nc-TiC/a-C coatings studied under similar conditions by Lewin et al. [2] is also included in Fig. 9. The nc-TiC/a-C coatings have a higher and rather constant resistivity compared to the nc-NbC/a-C coatings that increases rapidly with carbon content. A plausible explanation to the difference in resistivity is the higher amount of a-C matrix in the Ti-C system.

Fig. 10 shows contact resistances of three coatings deposited on Ni-coated cylinders. XRD and XPS of these coatings showed the same phase composition and structure, but a small difference in the amount of free carbon and grain size compared to the coatings deposited on the Si substrates. This can be explained by the condition that the samples were positioned at the edge of the sample holder during deposition. However, the trend of the amount of free carbon and grain size with composition is identical to the results in Figs. 4 and 6. The results in Fig. 10 clearly show that the contact resistance is strongly dependent on composition. The nc-NbC/a-C coating with 54 at.% C (38% a-C phase) and an intermediate grain size has the lowest contact resistance (140 μΩ at 100 N) while coatings with higher and lower carbon contents exhibited a higher contact resistance. A very similar trend in contact resistance has been observed for nc-TiC/a-C coatings deposited under similar conditions [2,16]. For both materials, the lowest contact resistance is obtained for carbon contents giving 30–40% a-C phase. This can be explained by a combination of electrical and mechanical properties. To have a low contact resistance, a surface oxide layer must be penetrated to enable electrical current to pass through the contact junction. The Nb – C coating containing 54 at.% C is richer in soft a-C phase and has smaller carbide grains than the metal rich coating containing 43 at.% C and should therefore be more ductile. This will improve the oxide penetration and hence give larger conductive contact area leading to a lower contact resistance. A further increase in carbon content increases the resistivity of the coating itself and thereby explains the higher contact resistance.

5. Conclusions

nc-NbC/a-C coatings have been deposited using DC magnetron sputtering. The size of nc-NbC grains and amount of a-C matrix phase can be controlled through the carbon content in the coatings. Although the amount of matrix phase increases with carbon content, a corresponding decrease in grain size leads to a more or less constant thickness of the matrix phase (Fig. 11). The contact resistance of the nc-NbC/a-C coatings strongly depends on composition and microstructure and the lowest value is found for the coating containing ~38% of a-C.

A comparison with the nc-TiC/a-C system shows that there is a weaker tendency to form a-C phase in the nc-NbC/a-C system resulting in less substoichiometric carbide grains ($TiC_{0.44–0.64}$ [2] compared to $NbC_{0.66–0.84}$) and a thinner a-C matrix. This difference strongly influences the coating properties. The electrical resistivity is lower for the nc-NbC/a-C coatings. In fact, the most Nb-rich coatings have about six times lower resistivity than corresponding nc-TiC/a-C coatings. The difference in thickness of the softer matrix phase can also explain the hardness difference. The results suggest that nc-NbC/a-C coatings have as good or better contact properties than nc-TiC/a-C. In fact, the lower resistivity, combined with a higher hardness and also a more oxidation-resistant behavior of Nb compared to Ti demonstrates that Nb-based contacts can have superior properties as electric contacts in a sliding application. Further studies in an oxidizing atmosphere at elevated temperatures are required, however, to evaluate the full potential of this material.

Acknowledgments

The authors acknowledge Vinnova (Swedish Governmental Agency for Innovation Systems) through the VINN Excellence Centre FunMat and project Designed Materials and Swedish Research Council (VR) for financial support.

References

[1] Å. Öberg, Å. Kassman, B. André, U. Wiklund, M. Lindquist, E. Lewin, U. Jansson, H. Högberg, T. Joelsson, H. Ljungcrantz, Eur. Phys. J. Appl. Phys. 49 (2010) 22902.
[2] E. Lewin, O. Wilhelmsson, U. Jansson, J. Appl. Phys. 100 (2006) 054303.
[3] P. Eklund, Surf. Eng. 23 (2007) 406.
[4] T. Zehnder, P. Schwaller, F. Munnik, S. Mikhailov, J. Patscheider, J. Appl. Phys. 95 (2004) 4327.
[5] D. Martinez-Martinez, C. Lopez-Cartes, A. Fernandez, J.C. Sanchez-Lopez, Thin Solid Films 517 (2009) 1662.
[6] C. Benndorf, M. Fryda, C.P. Klages, K. Taube, H.G. Haubold, Mater. Sci. Eng. A 140 (1991) 795.
[7] A.A. Voevodin, J.S. Zabinski, J. Mater. Sci. 33 (1998) 319.
[8] S. Zhang, X.L. Bui, J. Jiang, X. Li, Surf. Coat. Technol. 198 (2005) 206.
[9] D. Nilsson, F. Svahn, U. Wiklund, S. Hogmark, Wear 254 (2003) 1084.
[10] C. Benndorf, E. Boettger, M. Fryda, H.G. Haubold, C.P. Klages, H. Koberle, Synth. Met. 43 (1991) 4055.
[11] P. Eklund, J. Emmerlich, H. Hogberg, O. Wilhelmsson, P. Isberg, J. Birch, R.O.A. Persson, U. Jansson, L. Hultman, J. Vac Sci. Technol. B 23 (2005) 2486.
[12] W. Gulbinski, S. Mathur, H. Shen, T. Suszko, A. Gilewicz, B. Warcholinski, Appl. Surf. Sci. 239 (2005) 302.
[13] M. Stuber, H. Leiste, S. Ulrich, H. Holleck, D. Schild, Surf. Coat. Technol. 150 (2002) 218.
[14] E. Lewin, B. Andre, S. Urbonaite, U. Wiklund, U. Jansson, J. Mater. Chem. 20 (2010) 5950.
[15] E. Lewin, E. Olsson, B. André, T. Joelsson, Å. Öberg, U. Wiklund, H. Ljungcrantz, U. Jansson, Plasma Processes Polym. 6 (2009) S928.
[16] E. Lewin, Design of Carbide-based Nanocomposite Coatings, Acta Universitatis Upsaliensis, Uppsala, 2009, http://urn.kb.se/resolve?urn=urn:nbn:se:uu:diva-109427.
[17] Operator's Multipak Software Manual, Physical Electronics Inc., 2000.
[18] C.P. Kempter, E.K. Storms, R.J. Fries, J. Chem. Phys. 33 (1960) 1873.
[19] A. Guinier, X-ray Diffraction in Crystals, Imperfect Crystals and Amorphous Bodies, 2nd ed., W. H. Freeman & Company, San Francisco, 1963.
[20] G.K. Williamson, W.H. Hall, Acta Metallogr. 1 (1953) 22.
[21] J.F. Moulder, W.F. Stickle, P.E. Sobol, K.D. Bomben, Handbook of X-ray Photoelectron Spectroscopy, 3rd ed., Physical Electronics, Inc., Eden Prairie, 1995.
[22] L. Ramqvist, K. Hamrin, G. Johansson, U. Gelius, C. Nordling, J. Phys. Chem. Solids 31 (1970) 2669.
[23] P. Ettmayer, W. Lengauer, in: R.B. King (Ed.), Carbides: Transition Metal Solid State Chemistry, John Wiley & Sons Ltd., Chichester, 1994.
[24] L.E. Toth, Transition Metal Carbides and Nitrides, Academic Press, New York and London, 1971.
[25] A. Leyland, A. Matthews, Wear 246 (2000) 1.